Journal of Alloys and Compounds 517 (2012) 61–68

Contents lists available at SciVerse ScienceDirect

Journal of Alloys and Compounds

journal homepage: www.elsevier.com/locate/jallcom

Microstructural stability of ultrafine-grained niobium–zirconium alloy at elevated temperatures

F. Rubitschek[a,*], T. Niendorf[a], I. Karaman[b], H.J. Maier[a]

[a] Lehrstuhl für Werkstoffkunde, Universität Paderborn, Pohlweg 47-49, D-33098 Paderborn, Germany
[b] Texas A&M University, Department of Mechanical Engineering, College Station, TX 77843, USA

ARTICLE INFO

Article history:
Received 27 October 2011
Received in revised form
28 November 2011
Accepted 29 November 2011
Available online 9 December 2011

Keywords:
UFG
High-temperature fatigue
Recrystallization
Grain coarsening
Cyclic stability
Refractory alloys

ABSTRACT

The present study reports on microstructural evolution upon static annealing treatment and elevated-temperature low-cycle fatigue (LCF) of an ultrafine-grained (UFG) body-centered cubic (bcc) niobium–zirconium (NbZr) alloy, processed by equal channel angular processing (ECAP) at room temperature.

UFG NbZr showed recovery and recrystallization at homologous temperatures, which are in the same range as those of another UFG bcc material, i.e. interstitial free (IF) steel. Unlike the UFG IF steel, the UFG NbZr featured a distinct plateau of decreased hardness due to recovery at temperatures below the recrystallization limit. This was attributed to the absence of dynamic recovery during ECAP due to the low homologous temperature of $T_h = 0.11$ ($T_h = 0.16$ for IF steel) at room temperature processing.

Strain-controlled elevated-temperature LCF tests performed in vacuum revealed stable cyclic deformation response up to 600 °C ($T_h = 0.32$). At higher temperatures, but still below the static recrystallization limit (≈900 °C, $T_h = 0.43$), cyclic softening, rapid decrease of mean stress and premature failure were observed. As compared to the UFG IF steel, cyclic stability is preserved up to higher T_h due to the stabilizing effect of solid solution alloying elements, i.e. mainly Zr.

In the case of the UFG IF steel, localized grain coarsening at the crack tip caused premature failure upon elevated-temperature LCF below the static recrystallization temperature. The more stable microstructure in the UFG NbZr did not show any localized alterations in the vicinity of the crack tip, but instead slightly coarsened throughout the whole gauge length.

In combination with the results obtained on the UFG IF steel in previous studies, a comprehensive summary of the microstructural evolution of UFG bcc materials at elevated temperatures is presented.

1. Introduction

Ultrafine-grained (UFG) metals and alloys have been widely studied during the last decade, since they feature both higher strength and good ductility, as compared to their counterparts of conventional grain-size (CG). In most bulk UFG materials, this favorable combination of properties is introduced by severe plastic deformation (SPD) [1–7]. Among other SPD techniques, equal channel angular processing (ECAP) has proven suitable for creating relatively large volumes of homogenously deformed bulk UFG materials [2,3,8]. When efficient processing routes are used uniform microstructures are achieved, featuring equiaxed grains with average diameters in the sub-micron regime and a large fraction of high-angle grain boundaries (HAGBs) [9–11]. These characteristics promote nearly isotropic mechanical properties and high microstructural stability upon monotonic and cyclic loading [9,11–13].

However, a significant amount of energy is introduced into a material by SPD, causing instability of the UFG microstructure when distinct temperatures and strain amplitudes are exceeded during operation. These limits highly depend on the lattice structure and the chemical purity of the material investigated, as well as on the processing route, which determines the microstructural characteristics [9,12–15].

Above a critical temperature, recrystallization and grain growth may occur. Eventually, these mechanisms set an inherent upper limit to operating temperatures for SPD materials. Of course, they are not limited to UFG materials. However, the latter are usually more prone to grain coarsening at relatively lower temperatures since the activation energy for recrystallization is decreased by the high dislocation density present in typical SPD materials and the driving force for grain growth is high because of the high fraction of non-equilibrium grain boundaries [16]. Cyclic plastic deformation may similarly contribute to microstructural instability as additional energy is induced and strain localization may lead to

* Corresponding author. Tel.: +49 5251 60 5235; fax: +49 5251 60 3854.
E-mail address: felix.rubitschek@uni-paderborn.de (F. Rubitschek).

0925-8388/$ – see front matter © 2011 Elsevier B.V. All rights reserved.
doi:10.1016/j.jallcom.2011.11.150

dynamic recrystallization at temperatures significantly lower than those under static conditions [17–19].

Thermal stability of several UFG face-centered cubic (fcc) materials, especially Cu, Al and its alloys, has been studied in recent years. Also, cyclic deformation responses (CDRs) and their relation to microstructural features have been investigated for these materials [13,17,18,20,21]. However, for UFG body-centered cubic (bcc) materials, there is still a lack of knowledge regarding thermal stability and especially the effect of combined thermal and fatigue loading. In a previous study, the authors have investigated elevated-temperature fatigue behavior of UFG interstitial free (IF) steel and pointed out the microstructural mechanisms of cyclic softening at these temperatures [15]. In the present study, a comprehensive summary of microstructural evolution in UFG bcc materials at elevated temperatures under static and fatigue loading conditions is presented, combining the current results on UFG bcc NbZr and the previous results on UFG IF steel.

Two refractory niobium–zirconium (NbZr) alloys were investigated in the current study, which are both characterized by good ductility and excellent corrosion resistance in aggressive environments provided by a dense passive surface layer. Currently, NbZr alloys are often employed in nuclear power systems, but more recently, Nb-based alloys have been envisaged for biomedical applications due to their excellent biocompatibility [22–24]. The relatively low ultimate tensile strength in the CG condition is increased significantly from 250 MPa to 690 MPa by ECAP following route 16E[1] (NbZr alloy 1), without sacrificing ductility [25]. The two alloys investigated in the current study, which mainly differ in their Zr content, were chosen since the (thermal) stability of UFG fcc microstructures strongly depends on the content of alloying elements and impurities [18–20,26], and thus, the alloying content is expected to have a similar influence in UFG bcc materials as well.

Low-cycle fatigue (LCF) tests conducted in a previous study showed pronounced cyclic stability of the UFG NbZr for strain amplitudes up to 0.5% at room temperature (RT) [25]. Conventional Nb alloys are known to have favorable mechanical properties at elevated temperatures due to their high melting point. However, the stability of the UFG microstructure in NbZr at elevated temperatures has remained unexplored so far.

In order to shed light on this aspect, annealing treatments and elevated-temperature LCF tests in combination with subsequent microstructural investigations were performed.

2. Experimental procedures

The chemical compositions of the two NbZr alloys investigated are given in Table 1. Both were obtained as hot rolled plates. Billets with the dimensions of $25 \times 25 \times 175\ mm^3$ were cut from the plates by electro-discharge machining (EDM). Subsequent ECAP was performed at RT at a processing speed of 2.5 mm/s following the processing routes 16E (NbZr alloy 1) and 8E (NbZr alloy 2). The numerical characters of the routes denote the total number of processing passes while the alphanumerical characters indicate the rotation of the billets between two consecutive passes (route E processing schedule is a sequence of 180°/90°/180° rotations around the longitudinal axis). The ECAP tool used has a cross section of $25 \times 25\ mm^2$ with a sharp 90° angle die and benefits from the "sliding walls" concept [27]. For further information on ECAP, processing routes and their nomenclature, the reader is referred to [3,8].

Routes 16E and 8E have been chosen because they provide cyclically stable microstructures at room temperature with an equiaxed grain morphology and a high volume fraction of HAGBs. Moreover, using route E, relatively large volumes of homogenously deformed material can be extracted from the billets, as compared to other ECAP routes [8]. Irrespective of the higher number of passes, route 16E materials have demonstrated very similar microstructural and mechanical properties as route E with only 8 passes due to saturation effects [25,28].

All UFG NbZr specimens used in the present work were EDMed from the homogenously deformed volume of the ECAP billets and then ground in order to remove the EDM-affected surface layer. The static annealing specimens had a cuboidal shape with dimensions of $10 \times 5 \times 1.5\ mm^3$. Prior to annealing, each specimen was sealed in a silica glass tube in vacuum environment with a pressure of $p < 10^{-4}$ mbar in order to minimize oxidation processes. Heat treatments were performed, always for 1 h, at different temperatures ranging from 400 to 1200 °C in a furnace with subsequent cooling at ambient temperature. Prior to the hardness measurements, specimens were ground, starting with coarse 320 SiC paper in order to remove any potentially affected surface layer, down to a grit size of 5 μm. For the electron backscatter diffraction (EBSD) measurements, specimens were polished in an alternating process of mechanical polishing using 1 μm alumina suspension and chemical etching[2] at RT.

The dog-bone shaped specimens used for fatigue testing were also ground down to 5 μm grit size in order to provide for smooth unnotched surfaces. Fully reversed push–pull LCF tests were performed in an MTS servohydraulic testing rig equipped with a vacuum chamber. All tests were conducted in total strain control with a constant strain amplitude of 5×10^{-3} and a strain rate of $6 \times 10^{-3}\ s^{-1}$ using a high-temperature extensometer with ceramic rods and a gauge length of 12 mm. This specific strain amplitude was chosen since previous LCF studies have demonstrated cyclic stability up to that strain amplitude at RT. In addition, when taking into account the different Young's moduli, these test parameters were supposed to yield similar plastic strain amplitudes as those obtained on IF steel in [15]. In order to avoid buckling of the relatively thin specimens, tight brackets were attached. Specimens were heated using a high frequency induction generator and a copper coil, which was adapted to the specimens' geometry in order to provide for a homogenous temperature profile throughout the gauge section.

Temperature was controlled using a thermocouple spot-welded to the brackets. In order to obtain accurate specimen temperature levels, a calibration specimen equipped with three thermocouples in the center and at the ends of the gauge length had been used prior to fatigue testing, such that actual specimen temperature could be related to the temperature of the thermocouple at the brackets used for temperature control.

All fatigue tests were performed in vacuum at a pressure of $<10^{-5}$ mbar. Samples were heated within 60 s and tests were started directly after reaching steady state temperature in order to avoid microstructural changes prior to fatigue testing.

For subsequent EBSD microstructure analyses of the fatigued material, samples were cut from the center of the gauge section of the fatigue specimens, ground and polished the same way as described for the static annealing specimens.

TEM specimens were extracted from the same sections as those used for EBSD and mechanically ground down to 0.15 mm foil thickness. Large electron-transparent areas were obtained by ion milling with an inclination angle of ±4.5° on both sides of the specimen with 5.5 keV and 30 μA ion current. The milling affected surface layer was removed by a 1 keV and 5 μA ion beam. For the TEM investigations the microscope was operated at a nominal voltage of 200 kV.

3. Experimental results and discussion

3.1. Static annealing treatment

In Fig. 1 a comparison of hardness values after annealing treatments at different temperature levels is given for UFG NbZr and UFG IF steel. Above a critical temperature, hardness is significantly decreased – mainly due to (partial) recrystallization – in all three materials, before the final saturation hardness level is reached due to complete recrystallization. While different contents of alloying elements have shown to exert significant influence on the critical recrystallization temperature of other UFG materials due to their stabilizing effect on the microstructure [18], the critical levels in the present study are very similar for all three materials if homologous temperature is considered instead of absolute temperature values ($T_{h,critical} \approx 0.43$).

In the case of IF steel the hardness decrease at $T_h > 0.5$ is more pronounced than for the two NbZr alloys, which indicates the effectiveness of the solid solution hardening in the latter alloys. NbZr alloy 2 features higher hardness values than NbZr alloy 1 in both, UFG and recrystallized conditions. This effect could stem from either the different chemical composition or – in the UFG condition – from the processing route. In the case of the IF steel, however, different processing routes led to very similar hardness at all temperatures [15]. Hence, the differences observed in case of the NbZr

[1] Information on ECAP and its nomenclature is given in Section 2 and in [3,8].

[2] Etchant: 25 ml ethanol, 50 ml H_2O_2, 25 ml HNO_3, 1 ml HF.

Table 1
Chemical composition of the two NbZr alloys investigated, as determined using inductively coupled plasma-atomic emission spectroscopy.

	Zr (wt%)	Ta (wt%)	Fe (ppm)	C (ppm)	O_2 (ppm)	H_2 (ppm)	Nb
NbZr alloy 1	1.02	<0.01	<5	140	202	49	Balance
NbZr alloy 2	2.3	0.29	<5	63	44	76	Balance

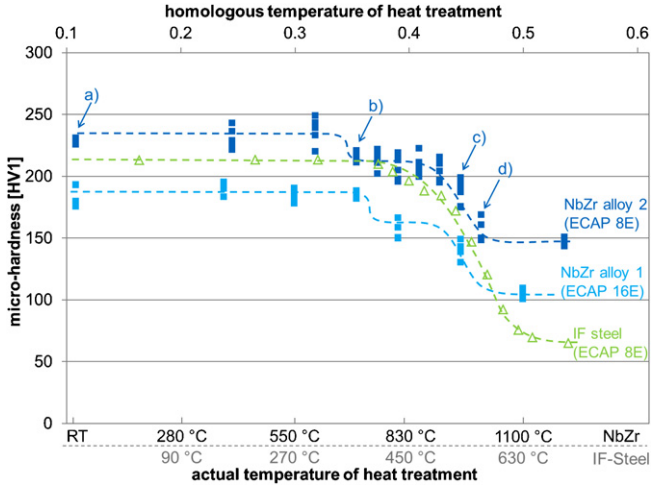

Fig. 1. Micro-hardness of UFG NbZr and UFG IF steel specimens after static annealing treatment for 1 h at various temperatures. The curves are plotted such that the upper scale bar shows homologous temperature for both, UFG NbZr and UFG IF steel, the corresponding actual temperature values for the different materials are given on the lower scale bar. Values for UFG IF steel were recompiled from [15]. The indicators a, b, c and d refer to the micrographs shown in Fig. 2.

alloys are attributed to the additional content of Zr and Ta and therefore a higher degree of solid solution hardening in the NbZr alloy 2.

Between $0.35 < T_h < 0.43$ a slightly decreased hardness plateau level is observed for the NbZr alloys, which is absent in the case of IF steel. The higher T_h during RT ECAP may induce dynamic recovery due to adiabatic heating during processing of the IF steel. Thus, no significant additional recovery is assumed upon further heat treatment. Because of its high melting point, NbZr is processed at relatively low T_h at RT so that no dynamic recovery is prevalent and a higher dislocation density remains after ECAP [25,28]. Therefore, during static annealing conducted below the recrystallization temperature, softening due to pronounced recovery is assumed to occur in UFG NbZr but not in UFG IF steel.

Fig. 2 shows different microstructures of UFG NbZr alloy 2 after annealing treatment at 700, 950 and 1000 °C and their respective grain size distributions. The corresponding hardness values are marked in Fig. 1. Despite the decreased hardness, grain size and overall appearance are not altered upon heat treatment up to 700 °C as compared to the 8E as-processed condition, clearly indicating that recovery is solely prevalent at this temperature.

At 950 °C a partly recrystallized microstructure is apparent as also shown by the shift of the grain size distribution curve towards larger grain sizes. At 1000 °C, near the lower saturation level of the hardness curve in Fig. 1, the largest mean grain size is observed, which is due to recrystallization and/or grain growth.

Although some residual fine grains remained in Fig. 2c and d, true bimodal structures, as observed in several other UFG materials after annealing in a suitable temperature range [29–31] leading to few coarse recrystallized grains in an overall UFG structure were, however, not observed in the current study.

3.2. Elevated-temperature fatigue

The cyclic stability of fcc UFG materials has been reported to significantly depend on the content of alloying elements and impurities [4,13,18]. The presence of precipitates, solid solution hardening elements or impurities contributes to microstructural stability in a similar way. The mobility of grain boundaries is impeded, such that cyclic softening due to grain coarsening is hindered and shifted to higher temperatures as compared to higher purity materials. A higher content of solid solution hardening elements promotes increased cyclic stability as shown e.g. for UFG AlMg0.5 and UFG AlMg2 [18].

When fatigued at different temperature levels, NbZr alloy 2 showed pronounced cyclic stability up to 600 °C, i.e. $T_h = 0.32$ (Fig. 3). Cyclic softening and reduced fatigue lives occurred upon increasing the temperature to 650 °C ($T_h = 0.34$) and above. This behavior clearly indicates the onset of microstructural changes and is therefore considered as instable although no grain coarsening was detected by EBSD.

Under similar loading conditions,[3] UFG IF steel did not show pronounced cyclic softening at any temperature level up to $T_h = 0.32$. However, already at a T_h of 0.26, fatigue life was reduced to less than 50% of fatigue life at room temperature and EBSD scans clearly revealed a coarsened grain structure, such that the microstructure of the UFG IF steel is considered as instable at that temperature level and above. Obviously, the solid solution hardening prevalent in UFG NbZr is more effective for stabilization of the microstructure than the small amount of carbides present in the UFG IF steel.

In the UFG NbZr, increased temperatures led to decreased cyclic stress levels. This behavior is common for most materials, however, in the case of UFG IF steel initial cyclic hardening led to the same saturation stress level at all temperatures over a wide T_h range between 0.16 and 0.32. The UFG NbZr did not show significant cyclic hardening during the first load cycles (Fig. 3), which again indicates the absence of process induced recovery during RT ECAP in UFG NbZr, whereas the higher T_h during RT processing of IF steel causes dynamic recovery and thus facilitates work hardening upon cyclic loading (c.f. inset to Fig. 3).

In addition to the CDR, mean stress evolution during cycling (Fig. 4) is a sensitive indicator for microstructural stability. Mean stresses generally evolve during fatigue in several UFG materials due to relaxation of internal stresses induced by SPD and microstructural rearrangement upon cyclic plastic deformation. In the case of UFG NbZr, maximum mean stresses of 100 MPa occurred, which were not relaxed in RT LCF. At higher temperatures, the lower initial mean stresses were completely relaxed. In the 600 °C test, mean stress evolution (Fig. 4) does already indicate some microstructural changes, which are not yet apparent in the CDR (Fig. 3). In the case of the UFG IF steel, similar mean stresses evolved at low T_h, but were relaxed rapidly even at RT, indicating again the inferior microstructural stability as compared to the UFG NbZr (c.f. inset to Fig. 4).

[3] The strain amplitude used for LCF of UFG IF steel was 2.8×10^{-3}. Taking into account the different Young's moduli of IF steel and NbZr (210 GPa vs. 85 GPa) and their similar monotonic strength, similar plastic strain amplitudes of $\Delta\varepsilon_{pl}/2 \approx 1.3 \times 10^{-3}$ were observed at RT in both cases [28,32,33].

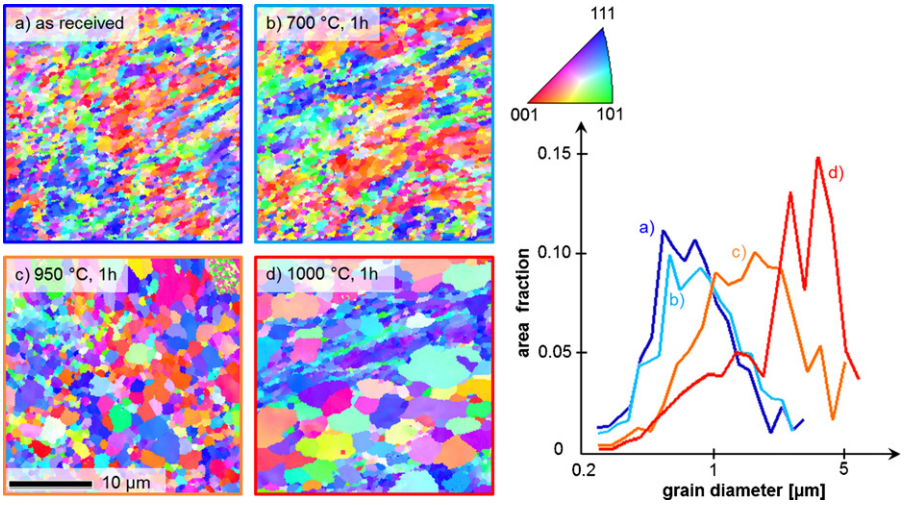

Fig. 2. EBSD micrographs depicting the microstructure evolution upon static annealing of UFG NbZr alloy 2 (a–d) and corresponding grain size distributions. Grain size remains unchanged up to 700 °C (b) as compared to the as-received condition (a). At 950 °C (c) and 1000 °C (d), the structures are (partly) recrystallized and average grain sizes are significantly increased.

The CDR of UFG NbZr alloy 1 at different temperatures is depicted in Fig. 5. As compared to alloy 2, the LCF behavior at all temperature levels was very similar. From RT up to 600 °C stable CDR is achieved, whereas 800 °C led to a similarly severe cyclic softening and premature failure as in alloy 2 (c.f. Fig. 3). Stress amplitudes of alloy 1 are clearly lower than those of alloy 2 which is in accordance with the inferior monotonic strength [25,33] and LCF responses at different strain amplitudes at RT.

The initial cyclic hardening during the first 80 cycles at 800 °C is similar to the behavior of UFG IF steel but unusual for UFG NbZr. This effect was reproducible and could stem from a combination of initial recovery before cycling followed by work hardening upon fatigue loading. However, the actual reason remains unclear.

The test at 800 °C was stopped prior to final failure, such that microstructural investigations could be performed in direct vicinity of the fatigue crack tip in order to reveal the mechanisms that led to the pronounced cyclic softening.

3.3. Microstructural characterization

In several UFG materials, grain coarsening is reported to be the dominant mechanism for cyclic softening, especially at elevated temperatures or when inefficient ECAP routes, leading to low-angle grain boundary dominated structures, are used [18,29]. While pure fcc UFG metals have a strong tendency to coarsen upon cyclic plastic deformation even at RT, UFG fcc alloys and UFG IF steel showed grain coarsening only at elevated temperatures, and in a localized form in the case of the UFG IF steel [15,18,20,29].

In order to clarify the dominating mechanism for UFG NbZr, EBSD measurements have been performed on selected conditions of UFG NbZr alloy 1 (Fig. 6). Obviously, the grain size in general is not altered upon fatigue at 800 °C (b), as compared to the as-ECAPed condition (a). According to Fig. 1, no grain coarsening is expected at this temperature level under static conditions. However, even moderate cyclic plastic deformation could contribute to

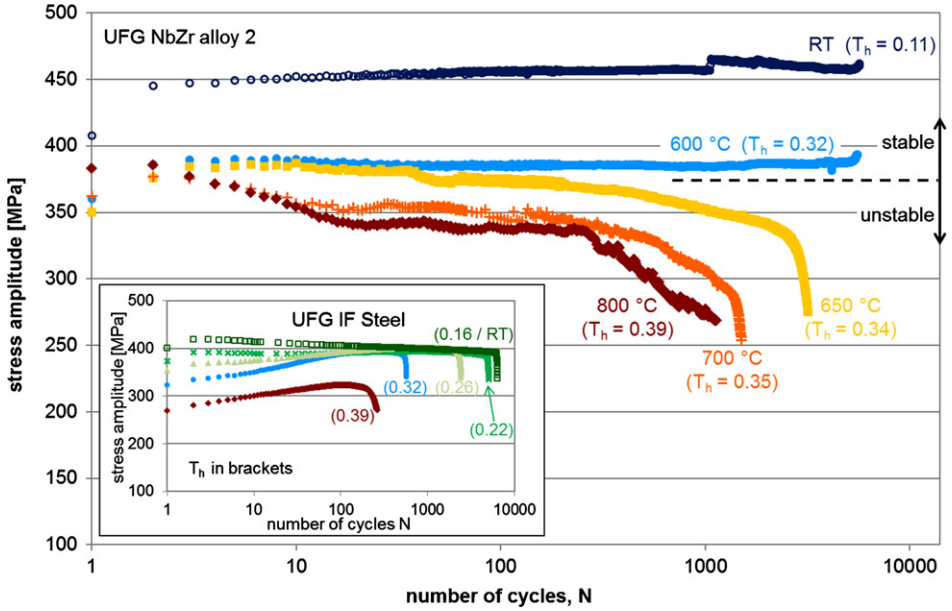

Fig. 3. Cyclic deformation response of UFG NbZr alloy 2 fatigue tested with constant $\Delta\varepsilon/2 = 0.5\%$ at various temperatures. Temperatures up to 600 °C yield stable cyclic responses, whereas cyclic softening is prevalent at temperature levels of 650 °C and above. The inset depicting the CDR of UFG IF steel was recompiled from [15].

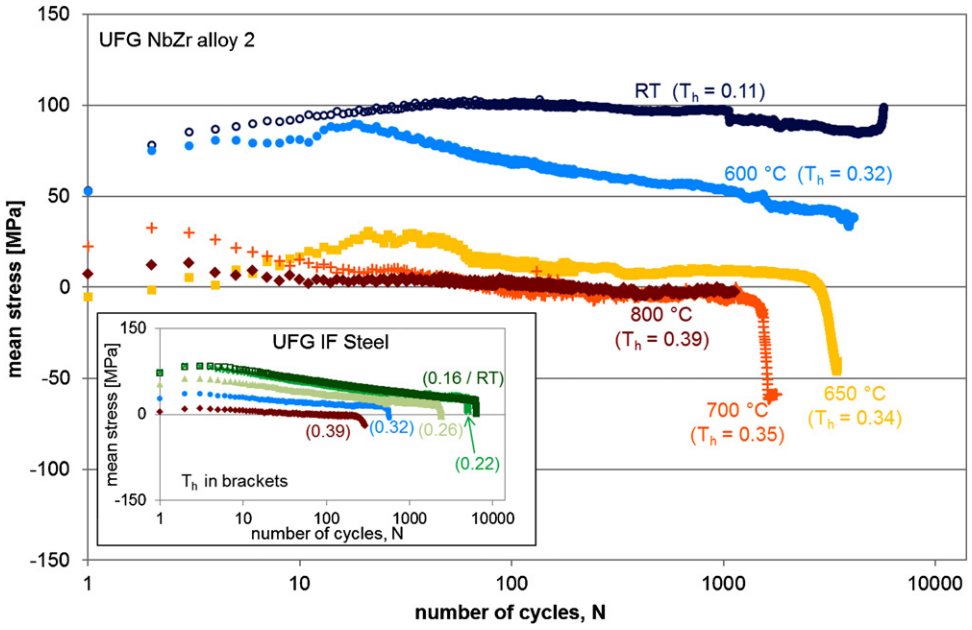

Fig. 4. Mean stress evolution upon elevated-temperature LCF of UFG NbZr alloy 2. Temperature levels of 650 °C and above, which are considered as cyclically unstable in Fig. 3, show rapid degradation of mean stress. The inset was recompiled from [15] and depicts the mean stress evolution of the UFG IF steel, corresponding to the inset of Fig. 3.

dynamic recrystallization such that coarsening might occur at significantly lower temperatures [15]. In the case of UFG IF steel, grain coarsening upon LCF was detected by EBSD at $T_h = 0.26$. By contrast, the current findings show that the microstructure of UFG NbZr is clearly more stable under similar LCF conditions as no significant grain coarsening is observed up to $T_h = 0.39$. While static recovery is clearly prevalent during the fatigue tests at the higher T_h (c.f. Fig. 1), pronounced cyclic softening at $T_h = 0.34$, which is right below the static recovery limit, does not occur before 1 h of test duration (≈1000 cycles). Therefore, dynamic recovery is assumed to be the main mechanism leading to cyclic instability in the UFG NbZr.

In order to get a more detailed insight into the microstructural evolution of the two UFG NbZr alloys, TEM investigations were undertaken on differently fatigued conditions (Fig. 7). Microstructures after RT LCF (Fig. 7a and b) are dominated by equispaced HAGBs, as also shown in a previous study [25], but are also characterized by grains with ill-defined contours containing a high amount of substructures and dislocations. As compared to the initial microstructures after ECAP, no fatigue-induced changes occurred [25]. Especially, grain coarsening due to dynamic recrystallization, as observed in several fcc UFG systems after strain-controlled LCF at RT, is absent [14,29,34]. This observation

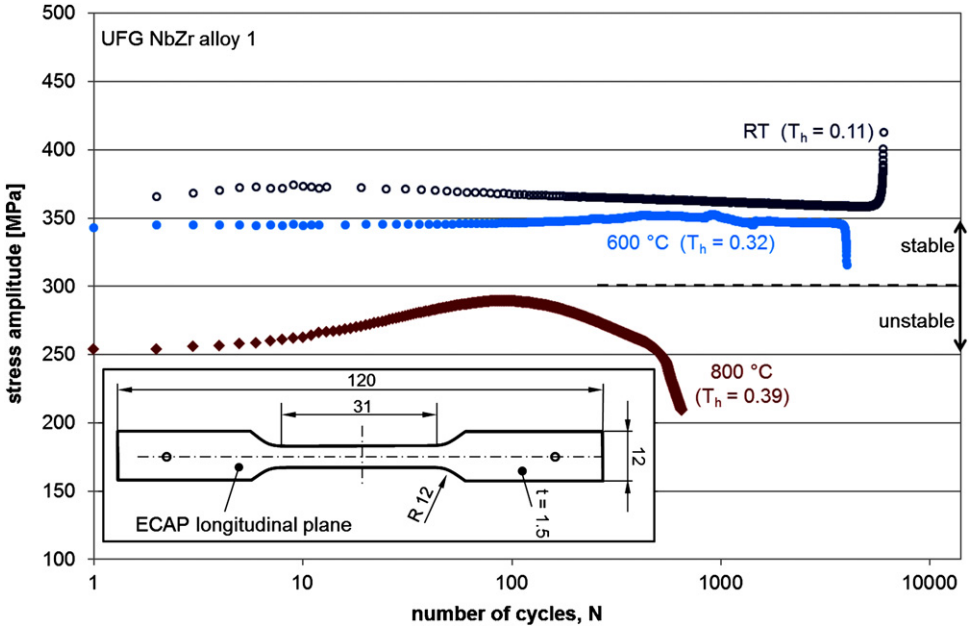

Fig. 5. CDR of UFG NbZr alloy 1 fatigued at constant $\Delta\varepsilon/2$ of 0.5% at various temperatures. At RT and 600 °C, a stable CDR is observed, while pronounced cyclic softening is prevalent at 800 °C. The inset depicts the specimen geometry used for all elevated-temperature LCF tests in the current study.

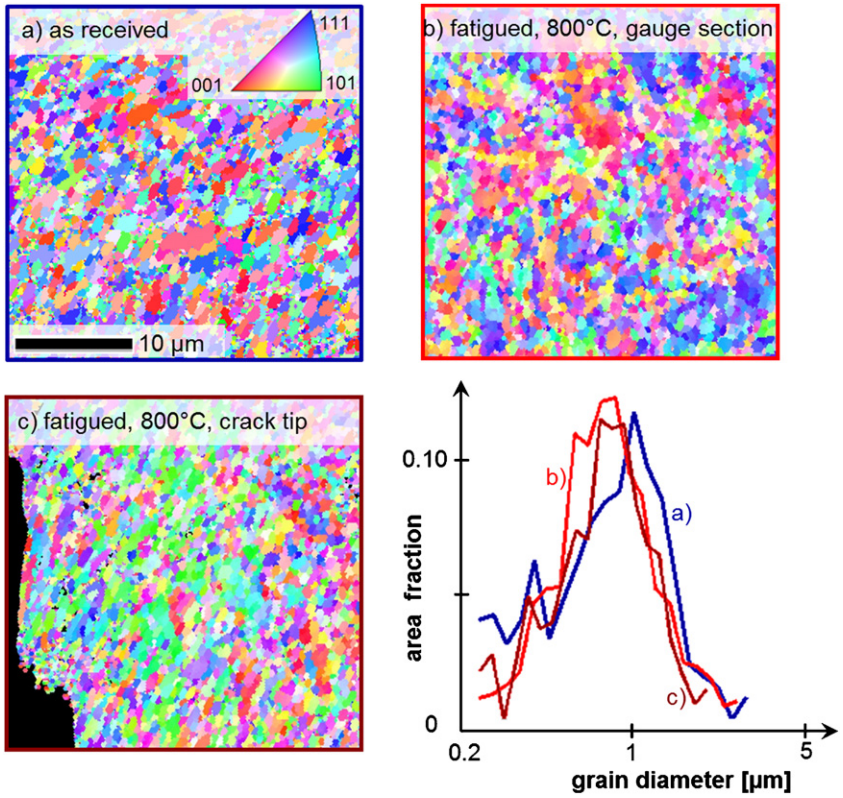

Fig. 6. EBSD micrographs with inverse-pole-figure mapping depicting the microstructure of UFG NbZr alloy 1 in (a) as-ECAPed condition, (b) fatigued condition after LCF at 800 °C; (c) originates from the same specimen as (b) but depicts the microstructure in the direct vicinity of the crack tip. The grain size statistics plot shows nearly identical distributions for all three cases.

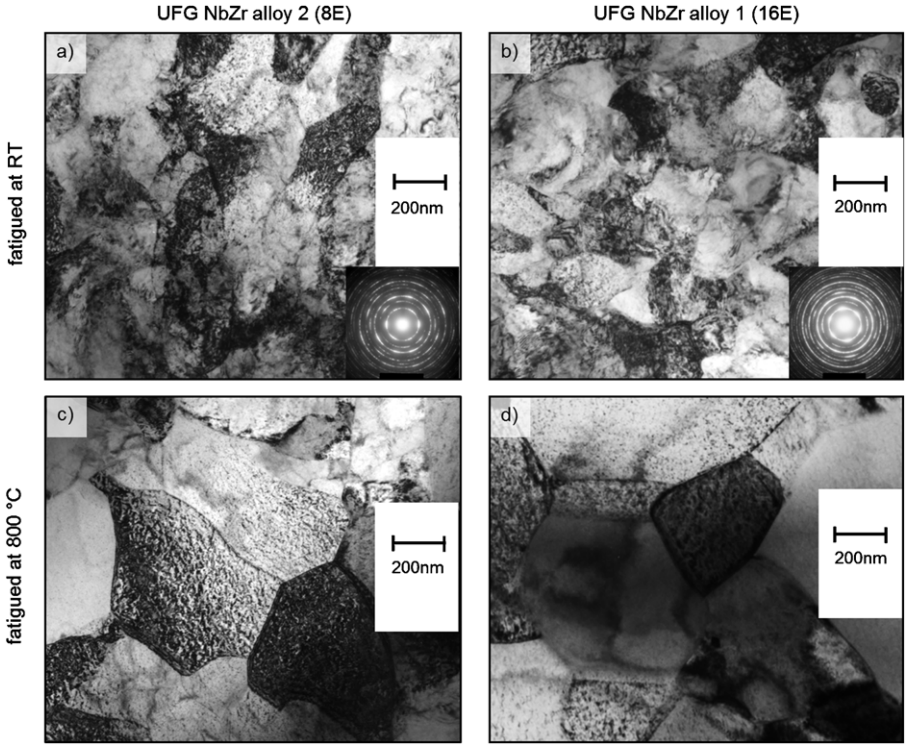

Fig. 7. TEM micrographs depicting the microstructure of UFG NbZr alloy 2 (a and c) and alloy 1 (b and d) in differently fatigued conditions. The images (a) and (b) refer to fatigue at RT and show microstructures that cannot be distinguished from the as-ECAPed condition. In (c) and (d), which refer to the condition fatigued at 800 °C, coarser (but still) UFG microstructures featuring a lower fraction of substructures have formed.

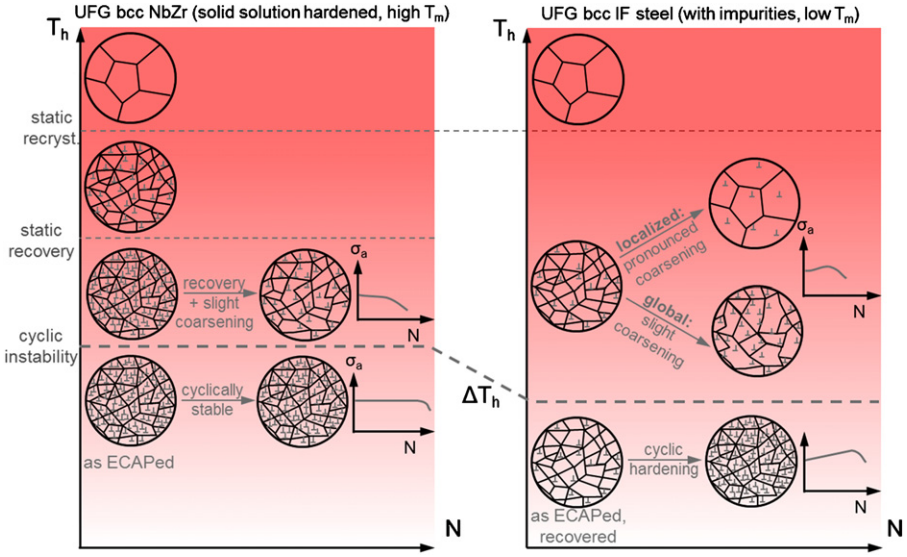

Fig. 8. Schematic summarizing the microstructural evolution during fatigue in the two investigated UFG bcc materials at different homologous temperature levels.

is in good accordance with previous investigations on UFG NbZr and holds true for UFG IF steel as well.

After fatigue at 800 °C, however, in both UFG NbZr alloys, apparently different microstructures as compared to the RT fatigue case have evolved. HAGBs are well-defined and most substructures have been dissolved. For that reason, the grains appear larger than those after RT fatigue. However, if only HAGBs are considered in both cases, the difference in grain size is minor. Clearly, even after fatigue at 800 °C, the average grain size remains in the UFG regime. As the EBSD technique (c.f. Fig. 6) does not reveal as fine details as the TEM, the current grain coarsening is apparently too weak to be detected by EBSD, but the microstructural changes can be clearly shown by TEM.

The deviation of grain sizes determined by EBSD and TEM, respectively, originates from their specific principles of operation. In the TEM, a high contrast is created by different crystallographic orientations and dislocations prevalent at grain boundaries, and very fine structural details can be imaged. By contrast, EBSD relies on diffraction information from a substantially larger volume. Clearly, different microstructural features are resolved by TEM and EBSD, which in turn can result in different grain size calculation [9].

As the TEM images do not show the direct vicinity of the fatigue crack, the coarsening appears to be a bulk phenomenon rather than a localized one. According to these findings, the microstructures in Fig. 7c and d can be considered as recovered and partly dynamically recrystallized, which would explain the cyclic softening and decreased fatigue life of UFG NbZr above a critical T_h of 0.39 as seen in Figs. 3 and 5.

Fig. 8 summarizes the findings of the current study and compares them to those obtained on the UFG IF steel. Microstructural evolution upon static heat treatment and fatigue loading is depicted, taking into account the different initial degree of recovery, the different temperature ranges of cyclic stability and the different types of coarsening, i.e. local vs. global, in cyclically unstable temperature ranges.

In the left part of Fig. 8 the characteristics of the solid solution hardened UFG NbZr with high melting point are outlined, the right part refers to the UFG IF steel, which is stabilized by impurities and characterized by a lower melting point. Starting from the as ECAPed condition (lower left), RT fatigue yields stable microstructures, which show no significant microstructural change in case of NbZr or cyclic hardening of the recovered structure (IF steel). Above a critical T_h the microstructures become cyclically unstable. This temperature is distinctly higher for NbZr (ΔT_h). Above the critical temperature, recovery and slight coarsening lead to cyclic softening in NbZr, whereas localized grain coarsening can occur in the IF steel. In the IF steel, cyclic hardening occurs at all temperature levels due to the presence of an initially recovered as-ECAPed structure. The latter also explains the absence of a distinct static recovery limit.

4. Conclusions

Static annealing and elevated-temperature fatigue tests were performed on two ultrafine-grained (UFG) niobium–zirconium (NbZr) alloys processed by equal channel angular processing (ECAP) using the efficient routes 8E and 16E. Microstructure investigations using electron backscatter diffraction and transmission electron microscopy were undertaken in order to clarify the dominant microstructural mechanisms in different temperature regimes. Results were discussed in combination with those obtained on UFG interstitial free (IF) steel in a previous study such that common mechanisms in bcc UFG materials are derived. The main findings are summarized as follows:

1. For UFG NbZr and UFG IF steel static recrystallization was found to occur at a very similar homologous temperature of $T_h \approx 0.43$, as determined by hardness measurements after static annealing. An intermediate plateau of slightly decreased hardness was observed in the two different NbZr alloys studied. This indicates the onset of recovery at temperatures slightly below recrystallization. This plateau was absent in case of UFG IF steel, indicating that dynamic recovery during ECAP was absent in UFG NbZr but occurred in the UFG IF steel due to the higher T_h during processing.
2. Elevated-temperature fatigue of UFG NbZr led to stable cyclic deformation response up to a T_h of 0.32. The transition to microstructural instability was observed at a critical T_h between 0.32 and 0.34, which is higher than in the case of UFG IF steel ($0.22 < T_{h,critical} < 0.26$) but still below the static recrystallization temperature. Above this temperature cyclic softening, rapid decrease of mean stresses and premature failure occurred. In contrast to the UFG IF steel, initial cyclic hardening did not occur, confirming the assumption that UFG NbZr was not recovered during ECAP because of the lower T_h during processing.
3. For the UFG IF steel localized coarsening at $T_h = 0.39$ led to cyclic instability. By contrast, localized coarsening was absent in case of

the UFG NbZr, as demonstrated by EBSD showing the microstructure in the vicinity of the fatigue crack. Instead, as shown by TEM images, a uniform rearrangement of low-angle grain boundaries, subgrains and dislocations along with slight grain coarsening occurred. Still, the grain sizes remained in the UFG regime.

Acknowledgements

The assistance of Mr. Philipp Krooß and Mr. Christian Rüsing with the experimental setup and the high-temperature LCF tests is gratefully acknowledged. Dr. Maik Häberlen is thanked for performing the ion milling process of the TEM specimens. Support from the National Science Foundation, International Materials Institutes Program through Grant No. DMR 08-44082, Office of Specific Programs, Division of Materials Research, Arlington, VA, USA, is acknowledged.

References

[1] V.M. Segal, Mater. Sci. Eng. A 197 (1995) 157–164.
[2] R.Z. Valiev, R.K. Islamgaliev, I.V. Alexandrov, Prog. Mater. Sci. 45 (2000) 103–189.
[3] R.Z. Valiev, T.G. Langdon, Prog. Mater. Sci. 51 (2006) 881–981.
[4] J. Horky, G. Khatibi, B. Weiss, M. Zehetbauer, J. Alloys Compd. 509 (Suppl. 1) (2011) S323–S327.
[5] G.I. Raab, R.Z. Valiev, T.C. Lowe, Y.T. Zhu, Mater. Sci. Eng. A 382 (2004) 30–34.
[6] A.V. Sergueeva, V.V. Stolyarov, R.Z. Valiev, A.K. Mukherjee, Scripta Mater. 45 (2001) 747–752.
[7] H.W. Höppel, J. May, M. Göken, Adv. Eng. Mater. 6 (2004) 219–222.
[8] R. Barber, T. Dudo, P. Yasskin, K.T. Hartwig, Scripta Mater. 51 (2004) 373–377.
[9] T. Niendorf, H.J. Maier, I. Karaman, D. Canadinc, Metall. Mater. Trans. A 38 (2007) 1946–1956.
[10] T. Niendorf, D. Canadinc, H.J. Maier, I. Karaman, G.G. Yapici, Scripta Mater. 58 (2008) 571–574.
[11] L. Saitova, H.W. Höppel, M. Göken, I.P. Semenova, G.I. Raab, R.Z. Valiev, Mater. Sci. Eng. A 503 (2009) 145–147.
[12] H.W. Höppel, M. Kautz, C. Xu, M. Murashkin, T.G. Langdon, R.Z. Valiev, H. Mughrabi, Int. J. Fatigue 28 (2006) 1001–1010.
[13] D. Canadinc, H.J. Maier, P. Gabor, J. May, Mater. Sci. Eng. A 496 (2008) 114–120.
[14] L. Kunz, P. Lukas, L. Pantelejev, O. Man, Procedia Eng. 10 (2011) 201–206.
[15] T. Niendorf, H.J. Maier, D. Canadinc, I. Karaman, Mater. Sci. Eng. A 503 (2009) 160–162.
[16] J. Lian, R.Z. Valiev, B. Baudelet, Acta Metall. Mater. 43 (1995) 4165–4170.
[17] H. Mughrabi, H.W. Höppel, M. Kautz, Scripta Mater. 51 (2004) 807–812.
[18] J. May, Mikrostruktur, monotone und zyklische mechanische Eigenschaften ultrafeinkörniger Aluminiumlegierungen, Dissertation, Erlangen-Nürnberg, 2008.
[19] W. Blum, Y.J. Li, K. Durst, Acta Mater. 57 (2009) 5207–5217.
[20] H. Hasegawa, S. Komura, A. Utsunomiya, Z. Horita, M. Furukawa, M. Nemoto, T.G. Langdon, Mater. Sci. Eng. A 265 (1999) 188–196.
[21] L. Kunz, P. Lukas, M. Svoboda, Mater. Sci. Eng. A 424 (2006) 97–104.
[22] R. Godley, D. Starosvetsky, I. Gotman, J. Mater. Sci. 15 (2004) 1073–1077.
[23] B. O'Brien, J. Stinson, W. Caroll, J. Mech. Behav. Biomed. Mater. 1 (2008) 303–312.
[24] G. Ramírez, S. Rodil, H. Arzate, S. Muhl, J. Olaya, Appl. Surf. Sci. 257 (2011) 2555–2559.
[25] T. Niendorf, D. Canadinc, H.J. Maier, I. Karaman, G.G. Yapici, Acta Mater. 55 (2007) 6596–6605.
[26] D. Canadinc, T. Niendorf, H.J. Maier, Mater. Sci. Eng. A 528 (2011) 6345–6355.
[27] V.M. Segal, R.R. Goforth, K.T. Hartwig, Apparatus and method for deformation processing of metals, ceramics, plastics and other materials, US Patent No. 5,400,633.
[28] T. Niendorf, D. Canadinc, H.J. Maier, I. Karaman, S.G. Sutter, Int. J. Mater. Res. 97 (2006) 1328–1337.
[29] H. Mughrabi, H.W. Höppela, M. Kautza, R.Z. Valiev, Z. Metallkd. 94 (2003) 1079–1083.
[30] H.J. Maier, P. Gabor, N. Gupta, I. Karaman, M. Haouaoui, Int. J. Fatigue 28 (2006) 243–250.
[31] T. Niendorf, D. Canadinc, H.J. Maier, I. Karaman, Int. J. Fatigue 30 (2008) 426–436.
[32] F. Rubitschek, T. Niendorf, H.J. Maier, I. Karaman, M. Haouaoui, Proceedings of the 6th International Conference on Low-cycle Fatigue, DVM, Berlin, 2008, pp. 313–318.
[33] F. Rubitschek, T. Niendorf, I. Karaman, H.J. Maier, J. Mech. Behav. Biomed. Mater. 5 (2012) 181–192.
[34] J. May, D. Amberger, M. Dinkel, H.W. Höppel, M. Göken, Mater. Sci. Eng. A 483–484 (2008) 481–484.